Journal of ELECTRONIC MATERIALS, Vol. 46, No. 2, 2017
DOI: 10.1007/s11664-016-5136-7
© 2016 The Minerals, Metals & Materials Society

X-ray Photoelectron Spectroscopy Study of Indium Tin Oxide Films Deposited at Various Oxygen Partial Pressures

SHOU PENG,[1,2,3] XIN CAO,[1,3] JINGONG PAN,[4] XINWEI WANG,[5] XUEHAI TAN ,[6,7] ALAN E. DELAHOY,[6] and KEN K. CHIN[6]

1.—State Key Laboratory of Advanced Technology for Float Glass, Bengbu Design and Research Institute for Glass Industry, Bengbu 233000, China. 2.—China Triumph International Engineering Co. Ltd., Shanghai 200063, China. 3.—School of Materials Science and Engineering, Dalian Jiaotong University, Dalian 116000, China. 4.—CNBM (Chengdu) Optoelectronic Materials Co. Ltd., Chengdu 610207, China. 5.—Evans Analytical Group, Liverpool, NY 13088, USA. 6.—CNBM New Energy Materials Research Center, New Jersey Institute of Technology, University Heights, Newark, NJ 07102, USA. 7.—e-mail: xtan@njit.edu

Here, a systematic experimental study on indium tin oxide (ITO) films is presented to investigate the effects of oxygen partial pressure on the film's electrical properties. The results of Hall measurements show that adding more oxygen in the sputtering gas has negative influences on the electrical conductivity of ITO films. As $O_2/(O_2 + Ar)\%$ in the sputtering gas is increased from 0 to 6.98%, the resistivity of ITO film rises almost exponentially from 7.9×10^{-4} to $4.1 \times 10^{-2}\ \Omega$ cm, with the carrier density decreasing from 4.8×10^{20} to 5.4×10^{18} cm^{-3}. The origins of these negative effects are discussed with focuses on the concentration of ionized impurities and the scattering of grain barriers. Extensive x-ray photoelectron spectroscopy (XPS) analyses were employed to gain insight into the concentration of ionized impurities, demonstrating a strong correlation between the oxygen vacancy concentration and the carrier density in ITO films as a function of sputtering O_2 partial pressure. Other microstructural characterization techniques including x-ray diffraction (XRD), high-magnification scanning electron microscopy (SEM) and scanning transmission electron microscopy (STEM) analyses were used to evaluate the average grain size of ITO films. For ITO films that have carrier density above 10^{19} cm^{-3}, scattering on grain boundaries and other crystallographic defects show negligible effects on the carrier transport. The results point to the oxygen vacancy concentration that dictates the carrier density and, thus, the resistivity of magnetron-sputtered ITO films.

Key words: ITO, magnetron sputtering, XPS, oxygen vacancy concentration, carrier concentration

INTRODUCTION

In the past decades, transparent conducting oxide (TCO) films, which transmit light and conduct electrical current simultaneously, are of increasing importance for various applications including optoelectronic and photovoltaic devices.[1-3] Recently, the world record of thin film solar cell conversion efficiency has been increased significantly.[4] Through the spectral quantum efficiency measurement and data analysis it was estimated that the most noticeable efficiency improvements have been originated from the development of a better superstrate, which includes a high-performance TCO layer,[5-7] a high-resistance transparent (HRT) layer[8,9] and a wide band gap buffer layer.[10-12] For a TCO layer that is used as the front contact of solar

(Received July 7, 2016; accepted November 10, 2016; published online November 28, 2016)

cells, its thickness can be substantially reduced with better electrical conductivity. This could potentially improve the short-circuit current density along with the filled factor, and, thus, enhance the conversion efficiency of a solar cell.

Among the large list of different TCO materials,[13-18] indium tin oxide (ITO) is one of the common materials because of its low resistivity, high transparency and good etchability.[19,20] While ITO films can be prepared from a wide range of deposition methods,[21-23] the most widely used fabrication technique for ITO films is magnetron sputtering directly from the ceramic target.[24,25] The electrical properties of ITO films depend on the sputtering conditions, such as the oxygen partial pressure.[26,27] Choi et al.[28] showed that both carrier mobility and concentration of ITO film decrease with increasing oxygen partial pressure, resulting in higher electrical resistivity. Kim et al.,[29] on the other hand, showed that carrier mobility of ITO film increases with oxygen partial pressure, leading to a decrease in electrical resistivity. A more recent study by Chen et al.[30] also visited such issues and showed that at higher oxygen partial pressure the carrier concentration increases but the carrier mobility decreases. Apparently, despite having been subject to extensive research, there is still a lack of consensus whether adding oxygen to the sputtering gas of Ar is beneficial to the electrical properties of ITO films. We believe more work can be useful to clarify such a point, maybe supporting one argument over another.

Herein, we intend to address the aforementioned issue by presenting an experimental study to compare the properties of ITO films deposited under pure Ar versus under different Ar-O_2 mixtures. The comparisons are performed systematically, with sputtering oxygen partial pressure being the only variable for our investigation. As will be demonstrated, higher oxygen partial pressure in the sputtering gas results in lower carrier density and concomitant deterioration in the electrical conductivity of ITO films. The origins of these negative effects are investigated using a variety of analytical techniques. X-ray photoelectron spectroscopy (XPS) is our primary tool, since ionized impurities could both serve as the doping agents and as the carrier scattering centers in a typical TCO material.[19] The analysis as a function of sputtering oxygen partial pressure provides evidence of correlation between the carrier density and the oxygen vacancy concentration of the ITO film. For films deposited at higher oxygen partial pressure, the diminishing oxygen vacancy concentration is responsible for the lower electrical conductivity.

MATERIALS AND METHODS

All ITO thin films were deposited on glass substrates by direct current (DC) magnetron sputtering (manufactured by SKY Technology Development Co., Ltd., model: K11-70) without any additional postdeposition annealing treatment. The sputtering power was fixed at 80 W, and the substrate temperature was maintained at 250°C for all depositions. The sputtering target was purchased containing 90 wt.% of In_2O_3 and 10 wt.% of SnO_2, according to the information provided by the manufacturer. To avoid variation in target composition, a single ITO target was used to deposit all films investigated in this study. The glass substrates were consistently cleaned before placement into the deposition chamber. A vacuum base pressure of 8×10^{-4} Pa or lower should be reached in the chamber before depositing the ITO films. During the deposition, argon and oxygen gases with purity of 99.999% were used at a working pressure of 0.4 Pa. While Ar flow rate was kept constant at 80 sccm, various oxygen flow rates, i.e. 0, 2, 3, 4, 5, and 6 sccm, were used for different sputtering gas mixtures, corresponding to an increasing ratio of O_2 flow rate over the total Ar-O_2 flow rates [O_2/(Ar + O_2)%] of 0%, 2.44%, 3.61%, 4.76%, 5.88%, and 6.98%, respectively. For simplicity, the ITO films deposited under these conditions were denoted as ITO-1 to ITO-6, respectively. Considering the sputtering gas mixture as an ideal gas, we have the equation of $P\,(\mathrm{d}V/\mathrm{d}t) = (\mathrm{d}n/\mathrm{d}t)\,RT$, where R is the ideal gas constant, and P, V, n, T are the pressure, volume, amount, and the absolute temperature of gas, respectively. Therefore, the flow rate of O_2 is proportional to its partial pressure, and the increasing O_2 flow rate at a fixed Ar flow rate can be described more generally as an increasing oxygen partial pressure. The sputtering rate was accurately measured *in situ* using a crystal monitor at the substrate plane. Additional *ex situ* calibrations were performed using a DekTak thin film thickness profiler (Veeco) to confirm the sputter rates employed and the resultant thicknesses. The thicknesses of all ITO films were fixed at 100 nm, unless otherwise stated.

The Hall effect measurements were performed in van der Pauw geometry at room temperature using the Ecopia HMS-3000 Hall measurement system. The film sheet resistance was measured using a four-point probe (Guardian) for quick checks of film conductivity. XPS measurements were performed on an ULTRA (Kratos Analytical) spectrometer under ultrahigh vacuum (10^{-7} Pa) using monochromated Al Kα radiation ($h\nu$ = 1486.6 eV) operated at 210 W. All XPS spectra were calibrated using the universal hydrocarbon contamination C 1s peak at 284.8 eV. X-ray diffraction (XRD) analysis was performed on a Bruker AXS diffractometer (Bruker Discover 8) using Cu Kα radiation (λ = 1.5406 Å) that was monochromated using a single Gobel mirror. The diffractometer was equipped with a Histar general area two-dimensional detection system (GADDs) with a sample-detector distance of 15 cm. For XRD grain size analysis, the instrumental broadening was carefully determined by using

LaB_6 standard material and subtracted from the measured line broadening. Scanning electron microscopy (SEM) analysis was performed with a Zeiss Sigma field emission scanning electron microscope operated at a 10-kV accelerating voltage. Focused ion beam (FIB) lift-out was performed on an FEI Helios 660 dual-beam FIB/scanning electron microscope to prepare the cross-section specimen for scanning transmission electron microscopy (STEM) analysis. Prior to introduction into the dual beam, a thin layer of ink was applied to the surface along with a thin sputter-coated Pt layer. Before milling, an FIB-deposited protective Pt-C layer was applied. The electron transparent cross-section specimen was imaged in a Hitachi HD2700 scanning transmission electron microscope operated at 200 kV.

RESULTS AND DISCUSSIONS

Figure 1 shows the results of Hall measurements on 100-nm-thick ITO films. It is found that adding more oxygen in the sputtering gas has negative influences on the electrical conductivity of ITO films. The measured resistivity of ITO film rises almost exponentially from 7.9×10^{-4} to 4.1×10^{-2} Ω cm with increasing oxygen partial pressure. Specifically, the carrier concentration of ITO films decreases from 4.8×10^{20} to 5.4×10^{18} cm^{-3} for $O_2/(O_2 + Ar)$% from 0% to 6.98%. The Hall mobility shows a general increasing trend from 17 to 45 $cm^2 V^{-1} s^{-1}$ for oxygen addition up to $O_2/(O_2 + Ar)$% of 4.76%; beyond that, the Hall mobility decreases and drops to a value of 28 $cm^2 V^{-1} s^{-1}$ at $O_2/(O_2 + Ar)$% of 6.98%. It should be mentioned that our results actually do not agree with any of the three works cited above.[28-30] Instead, our results are consistent with the findings of another work, in which the dependencies of resistivity, carrier density and mobility on oxygen deposition pressure were investigated for ITO films grown by pulsed laser deposition.[31]

Figure 2 shows the STEM micrographs for the cross-section of a typical ITO thin film deposited on glass substrate. For the purpose of STEM analysis, the thickness of this ITO film was selected to be 25 nm. The deposited film is polycrystalline with no or low evidence of amorphous phase. As shown by the high-resolution STEM micrograph inserted near the bottom, each ITO crystallite may actually occupy the entire film thickness. On the basis of this observation, we estimated the columnar grain structure from the faceted top surface, as sketched in the inserted micrograph near the top. We acknowledge that the columnar grain structure observed for 25-nm thick film may not represent the microstructure of thicker films. As described in the typical competitive van der Drift type crystallite growth that occurs during film deposition,[32,33] the grain probability of survival diminishes with increasing film thickness.

Figure 3a shows the results of XRD analysis on 100-nm films of ITO-1 to ITO-6. All films are polycrystalline single-phase solid solution with a body-centered cubic crystal structure [Ia-3 (206)]. There is no detectable variation in terms of the diffraction peak position. This may be consistent with the expectation that all six ITO films should, in principle, contain the same amount of Sn dissolved in the In_2O_3 lattice. As the oxygen partial pressure increases in the sputtering gas, the resulted ITO films become slightly more textured with a [222] preferred growth orientation. Close inspection of the XRD patterns reveals that there is diffraction peak broadening for ITO films deposited at higher oxygen partial pressure. Accordingly, we performed grain size analysis using Scherrer equation to estimate the average grain size of each film. As depicted in Fig. 3b, the average grain size of ITO film becomes gradually smaller with increasing $O_2/(Ar + O_2)$% in the sputtering gas. The trend of decreasing grain size can be confirmed by the results of SEM

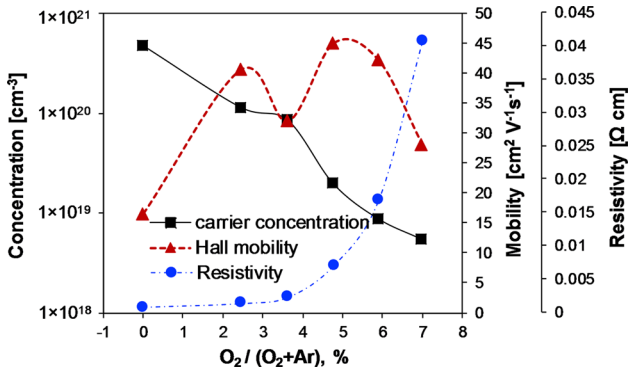

Fig. 1. Hall measurements. The carrier concentration, mobility, and resistivity of ITO films, plotted as a function of increasing $O_2/(Ar + O_2)$% in the sputtering gas.

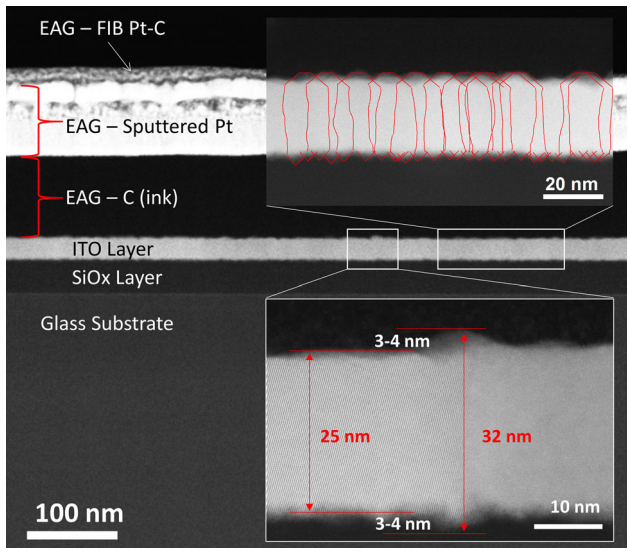

Fig. 2. STEM analysis. Cross-sectional view of a typical ITO thin film deposited on glass substrate. The inserts show the estimated columnar grain structure and the high-resolution micrograph

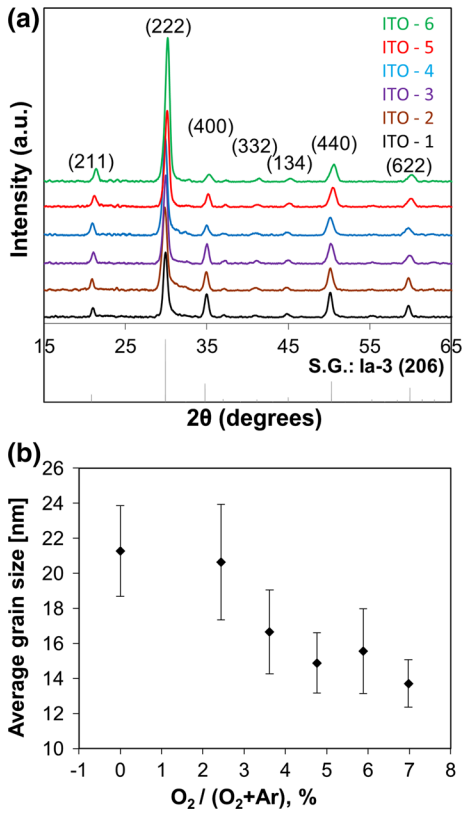

Fig. 3. XRD and grain size analysis. (a) XRD patterns of ITO films deposited under different oxygen partial pressures. (b) The grain size of ITO film as a function of $O_2/(Ar + O_2)$% in the sputtering gas; the error bars show the deviation from the mean.

analysis. The high-magnification SEM micrographs of the six ITO films are shown in Fig. 4.

From the results of Hall measurements, it is safe to argue that the lower electrical conductivities of ITO films deposited at higher oxygen partial pressure may be predominantly determined by their decreasing carrier concentrations. Comparing ITO-1 and ITO-6, their carrier concentrations are different by almost two orders of magnitude. The carrier concentration of ITO is determined by the extrinsic dopant Sn^{4+} ions and other intrinsic defects. At present, it is accepted by many researchers that oxygen vacancy is one of the fundamental sources acting as donors to produce carrier electrons in ITO and some other TCOs.[34-36] Here, we used XPS as our primary technique to analyze the bonding environment of In, Sn, and O. This allowed us to find the reason for the decreasing carrier concentration of ITO films deposited at higher oxygen partial pressures.

Figure 5a and b show the XPS spectra of In 3d, and Sn 3d, respectively, for ITO films that were deposited at different oxygen partial pressures. The doping efficiency of Sn^{4+} ions that substitute In^{3+} in the ITO lattice may vary with increasing oxygen in the sputtering gas. Earlier study using first-principles calculation has shown that even for cation site doping, an oxygen-poor growth condition is preferred to increase the dopant solubility.[37] Table I summarizes the quantitative analysis of the XPS spectra, focusing on the relative % of In, and Sn. The near-surface chemical compositions of all ITO films are, however quite consistent, showing In wt.% of 91.2±0.2%, and Sn wt.% of 8.8±0.2%. More importantly, chemical states of Sn^{0+} and Sn^{2+} are not detected for any ITO films examined here, and there is no evidence of diffraction peaks associated with the precipitated SnO_2 clusters, considering the results of XRD analysis shown in Fig. 3. Therefore, it may be safe for us to argue that the ionized impurity Sn^{4+} is not responsible for the decreasing carrier concentration of ITO films deposited at higher oxygen partial pressures. Interestingly, the spectrum of In or Sn is still required to be fitted with two components. While the major component corresponding to the valance state of In^{3+} (or Sn^{4+}), the minor component corresponds to a core level (CL) that actually has shifted to an even higher binding energy. A similar CL shift to a higher binding energy has been previously reported for Zn 2p XPS spectra of ZnO.[36] The component has been assigned to Zn^{2+} in the Zn-O bond but being surrounded by oxygen vacancies.

Figure 5c shows the XPS O 1s spectra of the ITO films that were deposited at different oxygen partial pressures. The O 1s spectra can be fitted with two components at ~529.8 eV, and ~531.4 eV.[38] The former component, labeled as O_I, represents oxygen ions that are surrounded by In or the substituted Sn atoms with their full complement of nearest-neighbor O^{2-} ions; the latter component, labeled as O_{II}, represents O^{2-} ions arising from the oxygen-deficient region, which may be connected in part to the oxygen vacancies.[39-41] As a result, comparing the ratio of integrated areas of O_{II} and O_I for different ITO films enables us to obtain a sensitive indicator of the variation of oxygen vacancy concentration.[39,41] It must be kept in mind that such a ratio does not represent the actual level of oxygen vacancies in ITO. The XPS O 1s spectrum should also contain components arising from the sample surface adsorption/contamination, but the amount of surface adsorption should be similar across all ITO films that were examined here. As shown in Fig. 6a, our results demonstrate a trend of decreasing oxygen vacancy concentration as a function of increasing $O_2/(O_2 + Ar)$%. An oxygen vacancy in the In_2O_3 lattice is known to generate two free electrons.[19] By plotting the ratio of O_{II}/O_I together with our data of carrier concentration, not in a log scale, the two sets of data actually have analogous variation trends as a function of $O_2/(O_2 + Ar)$%. This comparison provides strong evidence demonstrating the correlation between the oxygen vacancy concentration and the carrier density of the ITO films.

It is also noted from Fig. 5a and b that the minor component of In or Sn 3d spectra indeed diminishes in its area as a function of increasing oxygen partial pressure. This observation confirms their relationship with oxygen vacancy, and thus being

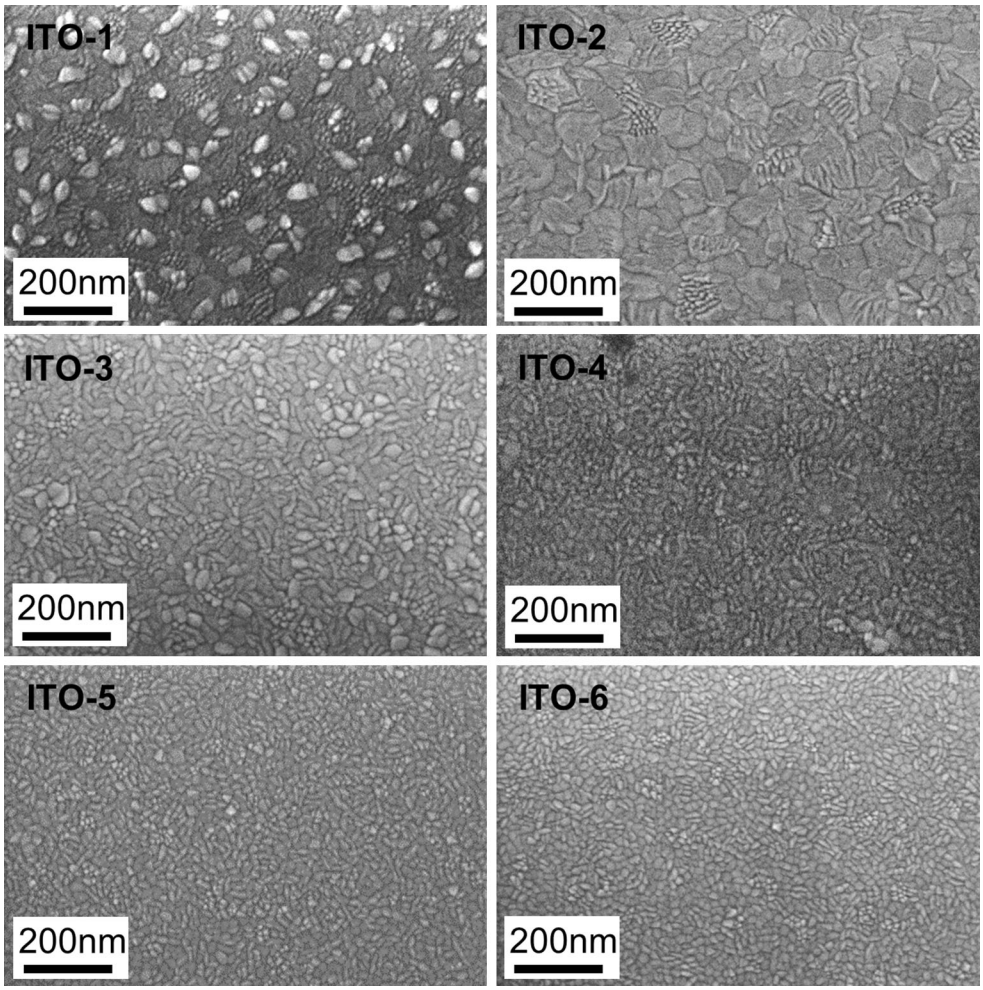

Fig. 4. SEM analysis. High-magnification SEM micrographs of ITO films. ITO-1 to 6 represent films deposited with $O_2/(Ar + O_2)$% of 0%, 2.44%, 3.61%, 4.76%, 5.88%, and 6.98%, respectively.

labeled as $In@O_{vac}$ and $Sn@O_{vac}$, respectively. By forming an oxygen vacancy in the oxide lattice, the remaining valance electrons, which were originally shared by In-O or Sn-O in the covalent bond, are now bonded much more weakly. During the XPS analysis, these electrons can be excited into the conduction band, and, consequently, the CL of In or Sn can shift towards a higher binding energy comparing to that of In^{3+} or Sn^{4+}. As shown in Fig. 6b, we have plotted the ratio of integrated areas for $In@O_{vac}/In^{3+}$ and for $Sn@O_{vac}/Sn^{4+}$ as a function of $O_2/(O_2 + Ar)$%. Both ratios are decreasing, but do not exactly follow the variation trend of carrier concentration or that of oxygen vacancy concentration. Probably, the arguments of oxygen vacancy concentration on the basis of In and Sn XPS spectra can be only taken with a grain of salt. However, from an overall viewpoint, our XPS results on O, In and Sn provide a consistent picture regarding the dependence of oxygen vacancy concentration on the sputtering oxygen partial pressure. This, in turn, predominantly determines the carrier concentration of the ITO films.

Carrier mobility is another important aspect of electrical conductivity that should be discussed. From Fig. 1, the variation of carrier mobility as a function of oxygen partial pressure is clearly not monotonic. The carrier mobility in polycrystalline degenerately doped semiconducting material is limited by several scattering mechanisms such as ionized impurity, lattice vibration, and boundary scattering.[42,43] By considering the boundary scattering that mainly occurs at grain boundaries and crystallographic defects, a decrease in grain size (shown in Figs. 3 and 4) should, in principle, result in higher probabilities of grain barrier scattering, leading us to expect a decrease in carrier mobility as the oxygen partial pressure increases in the sputtering gas. However, as shown in Fig. 1, the measured mobility data does not follow such expectation, at least for $O_2/(O_2 + Ar)$% up to 4.76%. This suggests that for high carrier concentrations, the change in grain size is not the predominant factor, or plays only a secondary role behind the observed trend of carrier mobilities.

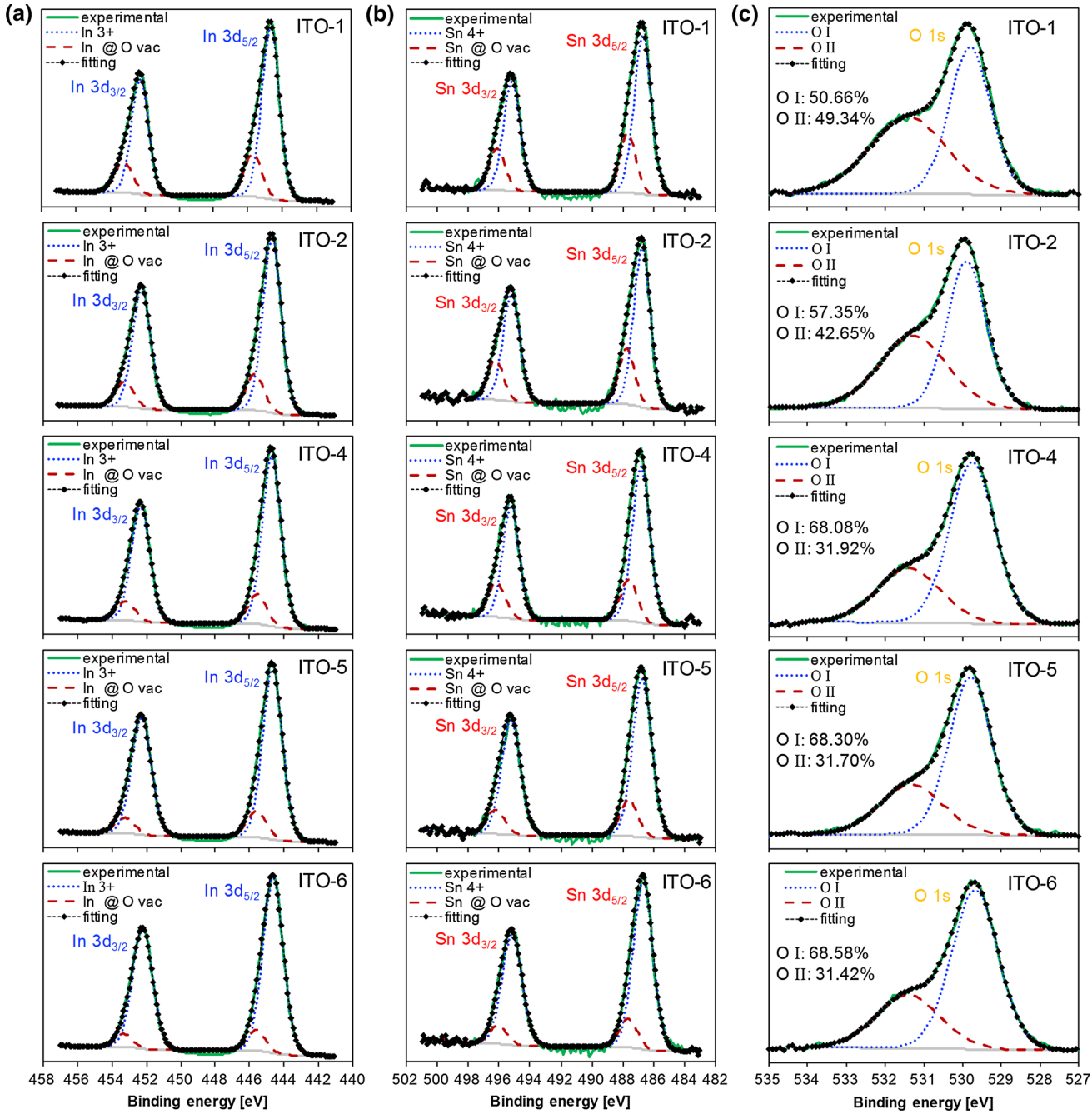

Fig. 5. XPS analysis. XPS spectra of (a) In 3d, (b) Sn 3d, and (c) O 1s for ITO films deposited at different oxygen partial pressures.

Table I. Quantitative analysis of the XPS results, summarizing In and Sn wt.% at the near-surface of ITO films

	ITO-1	ITO-2	ITO-4	ITO-5	ITO-6
In wt.%	90.9	91.4	91.2	91.4	91.1
Sn wt.%	9.1	8.6	8.8	8.7	8.9

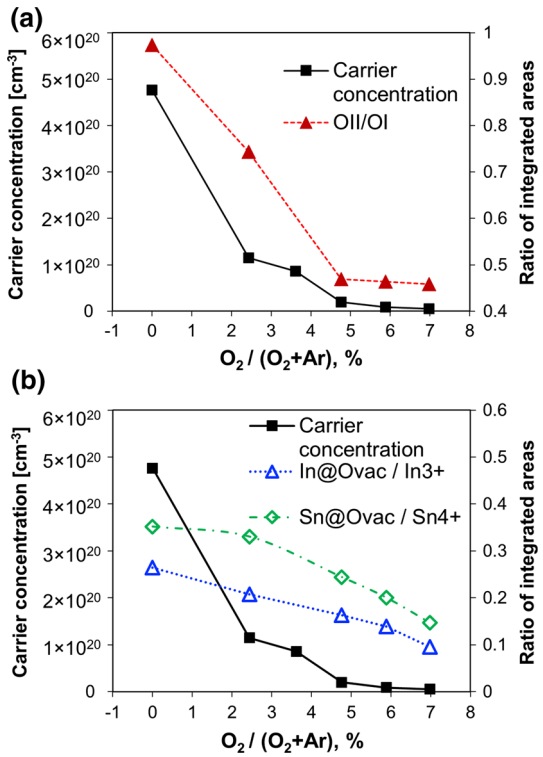

Fig. 6. Comparing (a) O_{II}/O_I, and (b) $In@O_{vac}/In^{3+}$ and $Sn@O_{vac}/Sn^{4+}$ with the data of carrier concentration shown in Fig. 1.

In addition, we compared the mean free path of electrons (l_e) with the average grain size. The mean free path for electrons in n-type degenerately doped semiconductor can be calculated using[14,44]:

$$l_e = \left(\frac{h}{2q}\right)\left(\frac{3n}{\pi}\right)^{\frac{1}{3}}\mu$$

where h is Planck's constant, q is the electron charge, n is the measured carrier concentration and μ is the measured Hall mobility. For ITO-1 to 4, the calculated values of l_e are 2.6, 4.0, 2.9, and 2.5 nm, respectively, all being considerably smaller than the corresponding grain size. These comparisons support our argument qualitatively. The grain barrier scattering only has minor/negligible effect on carrier transport for ITO films that have carrier concentration above 10^{19} cm^{-3}. Our argument is in accordance with the conclusions of an earlier study on carrier transport in various polycrystalline TCO films:[43] While grain barriers were found to limit the carrier mobility of ZnO with a carrier concentration of 2×10^{20} cm^{-3}, the influences due to grain barriers were not observed for ITO with a carrier concentration as low as $\sim 10^{18}$ cm^{-3}.

Finally, it is important to emphasize that while oxygen vacancy and Sn are the doping agents, they also serve as the scattering centers for carriers. At high carrier density, the charge carrier scattering processes due to ionized impurities should be the dominant mechanism limiting the mobility of our ITO films. Since oxygen vacancies are doubly charged, its scattering power is higher than that of singly ionized dopant Sn in ITO. As oxygen vacancy concentration decreases, the population of oxygen vacancy scattering centers reduces accordingly. This could explain our observation that the carrier mobility increases from ITO-1 to ITO-4, until the carrier concentration of ITO film reduces to a certain threshold. It is noted that further lowering of carrier concentration does not lead to higher mobility. Earlier study on ITO has shown that the onset of grain barrier limited transport, transiting from the ionized impurity limited transport, is on the order of 10^{18} cm^{-3}.[43] As carrier concentrations of ITO-5, and ITO-6 drop to the order of 10^{18} cm^{-3}, scattering on grain boundaries and other crystallographic defects becomes dominant, and the films show lower mobilities with reducing grain size.

CONCLUSION

In this study, we systematically clarified the influences of higher oxygen partial pressure on the electrical properties of ITO films deposited by magnetron sputtering. The film conductivity is negatively affected, because the carrier density of ITO films decreases dramatically with increasing oxygen partial pressure in the Ar-O_2 sputtering gas. The variation of carrier mobility is not monotonic. This is due to the combined effects of several charge carrier scattering mechanisms. We have demonstrated that there is a strong correlation between the carrier density and oxygen vacancy concentration in the ITO films. XPS analysis was employed as the primary technique to probe the oxygen-related defects. The oxygen vacancy concentration in the ITO films reduces progressively as the sputtering oxygen partial pressure increases. Our results clearly show that oxygen vacancy concentration plays an important role in determining the conductivity of magnetron-sputtered ITO films.

ACKNOWLEDGEMENTS

The authors acknowledge the China Triumph International Engineering Co. Ltd. (CTIEC), Shanghai, China, which offers generous financial support for this work. The authors thank the Evans Analytical Group's Materials Characterization Division for the FIB-STEM analysis.

CONFLICT OF INTEREST

The authors declare no competing financial interest.

REFERENCES

1. T. Minami, *Thin Solid Films* 516, 5822 (2008).
2. E. Fortunato, D. Ginley, H. Hosono, and D.C. Paine, *MRS Bulletin* 32, 242 (2007).
3. R.K. Pandey, S. Mishra, and P.K. Bajpai, *J. Electron. Mater.* 45, 5822 (2016).

4. M.A. Green, K. Emery, Y. Hishikawa, W. Warta, and E.D. Dunlop, *Prog. Photovolt: Res. Appl.* 24, 905 (2016).
5. A.E. Delahoy and S. Guo, *Handbook of Photovoltaic Science and Engineering*, ed. A. Luque and S. Hegedus (Chichester: Wiley, 2011), p. 716.
6. K. Jeyadheepan, M. Thamilselvan, K. Kim, J. Yi, and C. Sanjeeviraja, *J. Alloys Compds.* 620, 185 (2015).
7. Z. Ghorannevis, E. Akbarnejad, A. Salar Elahi, and M. Ghoranneviss, *J. Inorg. Organomet. Polym.* 25, 1486 (2015).
8. J.J. Wang, T. Ling, S.Z. Qiao, and X.W. Du *ACS Appl. Mater. Interfaces* 6, 14718 (2014).
9. J.L. Pena, E. Hernandez-Rodriguez, V. Rejon, R. Mis-Fernandez, and I. Riech, *PVSC IEEE 42nd* (2015). doi: 10.1109/PVSC.2015.7355894.
10. D.M. Meysing, C.A. Wolden, M.M. Griffith, H. Mahabaduge, J. Pankow, M.O. Reese, J.M. Burst, W.L. Rance, and T.M. Barnes, *J. Vac. Sci. Technol. A* 33, 021203 (2015).
11. D.A. Duncan, J.M. Kephart, K. Horsley, M. Blum, M. Mezher, L. Weinhardt, M. Haming, R.G. Wilks, T. Hofmann, W. Yang, M. Bar, W.S. Sampath, and C. Heske, *ACS Appl. Mater. Interfaces* 7, 16382 (2015).
12. J.M. Kephart, R.M. Geisthardt, and W.S. Sampath, *Prog. Photovolt: Res. Appl.* 23, 1484 (2015).
13. K. Ellmer, *Nat. Photonics* 6, 809 (2012).
14. Q. Gao, M. Li, X. Li, Y. Liu, C.L. Song, J.X. Wang, Q.Y. Liu, J.B. Liu, and G.R. Han, *J. Alloys Compds.* 550, 144 (2013).
15. Y. Zhu, R.J. Mendelsberg, J. Zhu, J. Han, and A. Anders, *J. Mater. Sci.* 48, 3789 (2013).
16. D. Panda and T.Y. Tseng, *J. Mater. Sci.* 48, 6849 (2013).
17. H. Mahdhi, Z. Ben Ayadi, J.L. Gauffier, and K. Djessas, *J. Electron. Mater.* 45, 557 (2016).
18. Y. Lu, S. Khan, C.L. Song, K.K. Wang, G.Z. Yuan, W. Li, G.R. Han, and Y. Liu, *J. Alloys Compds.* 663, 413 (2016).
19. T. Minami, *Semicond. Sci. Technol.* 20, S35 (2005).
20. T.H. Tsai and Y.F. Wu, *Microelectron. Eng.* 83, 536 (2006).
21. V. Linss, *Surf. Coat. Tech.* 290, 43 (2016).
22. S.M. Joshi and R.A. Gerhardt, *J. Mater. Sci.* 48, 1465 (2013).
23. M. Wegener, M. Kato, K. Kakimoto, S. Spallek, E. Spiecker, and A. Roosen, *J. Mater. Sci.* 50, 6124 (2015).
24. Y. Hu, X. Diao, C. Wang, W. Hao, and T. Wang, *Vacuum* 75, 183 (2004).
25. E. Terzini, P. Thilakan, and C. Minarini, *Mater. Sci. Eng. B* 77, 110 (2000).
26. F. Kurdesau, G. Khripunov, A.F. da Cunha, M. Kaelin, and A.N. Tiwari, *J. Non-Cryst. Solids* 352, 1466 (2006).
27. K.S. Tseng and Y.L. Lo, *Appl. Surf. Sci.* 285P, 157 (2013).
28. C.G. Choi, K. No, W.J. Lee, H.G. Kim, S.O. Jung, W.J. Lee, W.S. Kim, S.J. Kim, and C. Yoon, *Thin Solid Films* 258, 274 (1995).
29. Y.J. Kim, S.B. Jin, S.I. Kim, Y.S. Choi, I.S. Choi, and J.G. Han, *Thin Solid Films* 518, 6241 (2010).
30. A. Chen, K. Zhu, H. Zhong, Q. Shao, and G. Ge, *Sol. Energy Mater. Sol. Cells* 120, 157 (2014).
31. H. Kim, C.M. Gilmore, A. Piqué, J.S. Horwitz, H. Mattoussi, H. Murata, Z.H. Kafafi, and D.B. Chrisey, *J. Appl. Phys.* 86, 6451 (1999).
32. C. Ophus, E. Luber, and D. Mitlin, *Acta Mater.* 57, 1327 (2009).
33. C. Ophus, T. Ewalds, E.J. Luber, and D. Mitlin, *Acta Mater.* 58, 5150 (2010).
34. K. Okada, S. Kohiki, S. Luo, D. Sekiba, S. Ishii, M. Mitome, A. Kohno, T. Tajiri, and F. Shoji, *Thin Solid Films* 519, 3557 (2011).
35. J. Gwamuri, M. Marikkannan, J. Mayandi, P.K. Bowen, and J.M. Pearce, *Materials* 9, 63 (2016).
36. Y.Y. Chen, J.C. Hsu, C.Y. Lee, and P.W. Wang, *J. Mater. Sci.* 48, 1225 (2013).
37. C. Li, J. Li, S.S. Li, J.B. Xia, and S.H. Wei, *Appl. Phys. Lett.* 100, 262109 (2012).
38. S.V. Pammi, A. Chanda, J.K. Ahn, J.H. Park, C.R. Cho, W.J. Lee, and S.G. Yoon, *J. Electrochem. Soc.* 157, H937 (2010).
39. F.M. Simanjuntak, D. Panda, T.L. Tsai, C.A. Lin, K.H. Wei, and T.Y. Tseng, *J. Mater. Sci.* 50, 6961 (2015).
40. M. Chen, X. Wang, Y.H. Yu, Z.L. Pei, X.D. Bai, C. Sun, R.F. Huang, and L.S. Wen, *Appl. Surf. Sci.* 158, 134 (2000).
41. J.S. Kim, P.K.H. Ho, D.S. Thomas, R.H. Friend, F. Cacialli, G.W. Bao, and S.F.Y. Li, *Chem. Phys. Lett.* 315, 307 (1999).
42. T. Stapinski, E. Leja, and T. Pisarkiewicz, *J. Phys. D: Appl. Phys.* 17, 407 (1984).
43. K. Ellmer and R. Mientus, *Thin Solid Films* 516, 4620 (2008).
44. W. Wohlmuth and I. Adesida, *Thin Solid Films* 479, 223 (2005).